Electronic Supplementary Material (ESI) for Materials Horizons.

Supplementary Information

Homogeneous Gelation Leads to Nanowire Forests in the Transition Between Electrospray and Electrospinning

Lin Lei[a], Shensheng Chen[b], Catherine J. Nachtigal[a], Tyler F. Moy[b], Xin Yong[b], Jonathan P. Singer[a]*

[a]Rutgers University, Department of Mechanical and Aerospace Engineering, Piscataway, NJ, USA.
[b]Binghamton University, Department of Mechanical Engineering, Binghamton, NY, USA.

*Correspondence to: jonathan.singer@rutgers.edu

Methods and Materials

Precursor solutions

Methylcellulose (MC, 15 kDa, 17 kDa, 41 kDa, 63 kDa), polyethylene glycol 400 (PEG 400, average Mn 400 Da), ethylene glycol (EG), gelatin, Poly(N-isopropylacrylamide) (PNIPAAm), hydroxypropyl methylcellulose (HPMS) and LUDOX® TM-50 colloidal silica (50 wt% suspension in H_2O) were used as received from Sigma Aldrich. 50 nm PVP-capped gold nanoparticles were obtained from nanoComposix and used as received. The mixed solution of 60 wt% deionized water with 40 wt% Ethanol (Koptec, 200 proof pure ethanol) was used as the carrier solvent for the precursor solutions of electrospray deposition (ESD). The concentration of MC precursor solution was fixed at 1 wt% in water:ethanol mixed solution (60 wt%:40 wt%) and used for all parametric studies. Different ratios of MC with LUDOX®, EG and PEG 400 are used for adjusting the viscosity of MC, in order to investigate the wire formation behavior of MC with its blends. 50 nm gold nanoparticles were prepared with MC and MC:PEG 400 by keeping the concentration of total composition solids as 0.3 wt% in water:ethanol mixed solution (60 wt%:40 wt%). MC samples (flow rates, spray temperatures, molecular weights, spray distances and additive components series) and HPMS samples were prepared by keeping the concentration of total composite solids as 1 wt% in water:ethanol mixed solution (60 wt%:40 wt%), and the different solid loadings study was completed by varying the concentrations as 0.125 wt%, 0.25 wt%, 0.5 wt%, 1 wt%, and 2 wt%. Gelatin and PNIPAAm samples were sprayed from 0.25 wt% precursor solutions. The different ratios of MC:EG, MC:PEG 400, MC:50 nm gold nanoparticles and MC:LUDOX® blends were 0:1, 2:1, 5:1, 1:1, 1:2, 1:5, 1:0 by mass.

Electrospray setup

Electrospray was conducted as described previously[1]. The set up includes the following five main parts: a syringe pump, a stainless steel needle (Sai Infusion, 20 gauge, 1.5”), and a steel focusing ring (inner diameter of 2 cm and an outer diameter of 4 cm) were connected with two high-voltage power supplies (Matsusada Precision Inc. RB30-30P), and a 10 cm circular collection silicon wafer was placed on a hotplate. The focusing ring was positioned 1 cm above the spray needle in all but the tree spray in Fig. 5c. A disposable syringe (5 mL NORM-JECT®) was used for delivering spray solution which passes through the conductive needle with high voltages to produce sprays. The silicon wafer was clipped with a ground wire during spray. Silicon wafers and chips were cleaned and degreased by acetone and ethanol before spray.

Spray conditions

Taylor-cone jet sprays were achieved for all experiments in this study. The humidity was controlled between 55%-70% for each spray. All samples except the spray distances series were conducted using 6.2 kV as the driving voltage and the focus voltage was kept between 2.4 kV to 3.8 kV. The 3D coating of the Thoweil Hinoki Cypress was sprayed at 7.4 kV without the focus ring. Spray distance was fixed as 4 cm from spray needle to collection substrate. 30 °C, 50 °C, 70 °C, 90 °C, and 110 °C were used for the spray substrate temperature series, all samples were sprayed for 30 min and used a flow rate of 0.25 mL/hr. For the flow rate and spray time series, the spray substrate temperature was 90 °C. 0.02 mL/hr, 0.05 mL/hr, 0.15 mL/hr, 0.25 mL/hr, and 0.35 mL/hr were employed for making different flow rates samples, and sprayed total solids were kept as constant by varying spray time. For the time series study, 15 min, 30 min, 60 min, 90 min and 120 min were selected as spray times and the flow rate was 0.25 mL/hr. The spray distances series was prepared at a distance of 7 cm, 6 cm, 5 cm, and 3 cm by adjusting the spray

voltage to obtain a stable spray at a similar voltage over distance (an effective field strength). For the blends study of MC with LUDOX®, EG and PEG 400, all samples were collected at 0.25 mL/hr with the spray distance of 4 cm and spray substrate temperature of 90 °C. MC:PEG 400 samples were sprayed for 30 min, and the MC:LUDOX® and MC:EG samples were sprayed for 60 min. 50 nm gold nanoparticles with MC and MC:PEG 400 composites were prepared at 0.15 mL/hr with a spray distance of 4 cm for 30 min and a spray substrate temperature of 90 °C. PNIPAAm, gelatin and HPMS samples were sprayed at 0.10 mL/hr with a spray distance of 4 cm for 30min, and spray substrate temperatures of 25 °C, 60 °C, and 90 °C. The hole array was prepared with MC and MC:PEG 400 (5:1) at the flow rate of 0.25 mL/hr for 5.5 hr with ~ 40% humidity. The spray voltages were 8.0 kV and 8.3 kV respectively, and the spray temperature was 90 °C. The hole depth array consisted of a 2.5 cm stainless steel cube with 16 holes of diameter 0.3175 cm and depths ranging from 0.05-0.81 cm placed on a silicon wafer clipped with a ground wire on a heating plate. The spray needle was placed 4 cm from the hole array horizontally and 6 cm vertically. The 3D coating of Thoweil Hinoki Cypress was completed by using 1 wt% 5:1 (5:1) (MC:PEG 400) : 50 nm gold nanoparticles in 60 wt%:40 wt% weight-basis water:ethanol at 25 °C, with a spray flow rate of 0.20 mL/hr for 30 hr and humidity of ~40%. The spray voltage was 7.4 kV and the spray needle placed 4 cm above the tip of the tree vertically and 3 cm behind the tree horizontally.

Sample characterization

The morphologies of sprayed thin films were characterized by a Zeiss Sigma Field Emission Scanning Electron Microscope using in-lens imaging for single wire images and backscattering imaging at a 45-degree angle for cross-sectional images. For thickness measurements of the hole

array, samples were smoothed in water vapor by placing in and removing from a refrigerator, whereby the coatings were smoothed by condensation of ambient humidity. A microscopic reflectometer (Filmetrics F40EX) with a custom motorized stage (Zaber E13F33E) and mapping software were used for measuring thickness of thin films.

Dissipative particle dynamics simulation

We exploit dissipative particle dynamics (DPD) coupled with electrostatic calculations to uncover the dynamics and morphological evolution of highly charged polymeric droplets in ESD. The focus of computational modeling is to provide insight into the coupling of solvent evaporation, charge dynamics, and polymer/solvent transport that determines the final morphology of the deposit. DPD is an off-lattice particle method that is widely used to model complex fluidic systems on the mesoscale[2–4]. In DPD, each spherical bead represents a group of small molecules, whose dynamics is governed by Newton's second law. The nonbonded interactions between beads i and j include three components: conservative force, dissipative force, and random force. The total force on bead i is thus obtained as $\boldsymbol{F}_i = \sum(\boldsymbol{F}_{ij}^{\mathrm{C}} + \boldsymbol{F}_{ij}^{\mathrm{D}} + \boldsymbol{F}_{ij}^{\mathrm{R}})$. To reduce computational cost, similar to other particle-based simulations, the summation of nonbonded interactions in DPD runs over only neighbors within a certain cutoff radius r_c from the reference bead i.

The conservative force is given by a soft-core repulsion as $\boldsymbol{F}_{ij}^{\mathrm{C}} = a_{ij}(1 - r_{ij})\boldsymbol{e}_{ij}$, where a_{ij} is the maximum repulsion between beads i and j; $r_{ij} = |\boldsymbol{r}_i - \boldsymbol{r}_j|/r_{\mathrm{c}}$ is the inter-bead distance normalized by the cutoff radius; $\boldsymbol{e}_{ij} = (\boldsymbol{r}_i - \boldsymbol{r}_j)/|\boldsymbol{r}_i - \boldsymbol{r}_j|$ represents the force direction. The interaction strength between beads of the same species is set to 25 to reproduce the compressibility of water. The miscibility of different fluid components is controlled by an excess repulsion defined

as the difference between the cross-species repulsion and the same-species repulsion. The magnitude of excess repulsion can be quantitatively related to the interfacial tension between incompatible fluids through mapping to the mean-field Flory-Huggins theory[2,5–7]. A large value of excess repulsion leads to the phase separation of two fluids. The dissipative force $\boldsymbol{F}_{ij}^{\mathrm{D}}$, determined by the relative velocity of two beads $\boldsymbol{v}_{ij} = \boldsymbol{v}_i - \boldsymbol{v}_j$, is given by $\boldsymbol{F}_{ij}^{\mathrm{D}} = -\gamma w_D(r_{ij})(\boldsymbol{e}_{ij} \cdot \boldsymbol{v}_{ij})\boldsymbol{e}_{ij}$. The random force is given by $\boldsymbol{F}_{ij}^{\mathrm{R}} = \sigma w_R(r_{ij})\xi_{ij}\boldsymbol{e}_{ij}$. ξ_{ij} is a random variable with Gaussian statistics $\langle \xi_{ij}(t) \rangle = 0$ and $\langle \xi_{ij}(t)\xi_{i'j'}(t') \rangle = (\delta_{ii'}\delta_{jj'} + \delta_{ij'}\delta_{ji'})\delta(t - t')$. w_{D} and w_{R} are arbitrary weight functions depending on the interparticle distance. γ determines the strength of viscous dissipation and σ is the noise amplitude. The temperature of a DPD system T is controlled inherently through the fluctuation-dissipation theorem given that $\left[w_{\mathrm{R}}(r_{ij})\right]^2 = w_{\mathrm{D}}(r_{ij}) = \left(1 - r_{ij}\right)^2$ and $\sigma^2 = 2k_{\mathrm{B}}T\gamma$, with k_{B} being the Boltzmann constant. The dissipative and random forces are adopted from Brownian dynamics but modified into symmetric pairwise forms so that the total momentum of the system is conserved. In this manner, the hydrodynamic interactions can be properly reproduced in the DPD simulations[8–10]. The DPD simulations commonly use the cutoff radius r_{c} and the energy of thermal fluctuation $k_{\mathrm{B}}T$ to define the characteristic length and energy scales, respectively, while considering all beads having the same mass m. Based on the dimensional analysis, the characteristic time for DPD is thus given as $\tau = \sqrt{mr_{\mathrm{c}}^2/k_{\mathrm{B}}T}$. We present the simulation results in reduced units with r_{c}, m, and $k_{\mathrm{B}}T$ all set to 1, which also yields $\tau = 1$.

Electrostatic interactions in DPD

Sprayed droplets acquire significant net charge in ESD. Therefore, long-range electrostatic interactions must be explicitly incorporated to accurately predict the dynamics and deformation of

droplets. We applied a particle-mesh method to model the evolution of electric field and compute the electrostatic interactions between charged components[11–13]. Briefly, the electrostatic interactions are considered among off-lattice DPD beads that carry charges, but the calculation of electric field and force is performed on a square mesh overlaying with the simulation domain[14]. The point charge of a DPD bead is carefully distributed to their nearby mesh nodes so that the center of partial charges on the nodes coincides with the bead position. The smeared charge distribution prevents catastrophic binding of oppositely charged ions subject to DPD repulsion that is only soft-core. The electric force applied on the charged bead is then obtained by solving the nondimensional Poisson equation on the mesh by the finite difference discretization and the real-space successive over relaxation (SOR) method. The red-black SOR method is applied to parallelize the Poisson solver for simulating large-scale systems[12]. Notably, our electrostatic solver can readily define the dielectric constant of each fluid phase and thus capture the effect of dielectric contrast across a fluid-fluid interface, which is important for simulating a charged droplet suspended in air. The details of the electrostatic calculation are described in our previous work[11,12].

Charged polymer droplets

We modeled the net charge carried by a polymeric droplet as explicit ion beads. The discrete treatment of charge is not only fully compatible with the particle-nature of DPD, but also couples the movement of ions driven by fluid flow with its dynamics in the electric field. The initial configuration of the droplet was constructed as a spherical domain of radius 20, which was filled with a mixture of aqueous solvent, polymer, and ion beads. The initial number concentrations of solvent, polymer, and ion are 90.0%, 9.75% and 0.25%, respectively. An individual monodisperse polymer chain was modeled as a sequence of $N_\mathrm{p} = 200$ DPD beads connected by harmonic bonds.

Thus the polymer beads experience additional bond force given by $\boldsymbol{F}_{\mathrm{b}} = -k(r_{ij} - b)\boldsymbol{e}_{ij}$ with $k = 64$ being the spring constant and $b = 0.5$ being the equilibrium bond length. The droplet was placed at the center of a $60 \times 60 \times 60$ simulation box and surrounded by air beads. The average number density was 3 for both the droplet and air phases and the total bead number of the droplet was 100,480.

Simulation parameters

The interaction strength among all components within the droplet were all set to $a_{ij} = 25$ to model a homogeneous polymer solution that is sprayed. The air beads interact with the solvent and polymer beads unfavorably, with the parameters being $a_{\mathrm{vw}} = a_{\mathrm{vp}} = 100$ to capture the surface tension of the droplet. Each ion bead carries a charge of 0.5, which makes the charge density of the droplet to be 0.125%. Although a charge per bead of unity is typically used in previous DPD studies[14,15], we set the charge per ion bead to 0.5 to prevent unphysical behavior of ion beads across the droplet-air interface. The dielectric contrast across the interface of aqueous droplet and air influences the electrostatic interaction. For simplicity, the relative permittivity ratio between the droplet and air phase was set to 100 in the Poisson solver to properly capture the effect of dielectric contrast.[11] The interaction strength between the air and ion beads was set to a very high value of $a_{\mathrm{vc}} = 1000$ to ensure the ion beads are confined inside the droplet at the early stage of evaporation. All simulations ran 10,000 time steps for equilibrium before turning on electric field, the time step of the simulations was set to 0.04.

Evaporation model

To model evaporation, we gradually deleted solvent beads located at the droplet surface to model the escape of the solvent molecules from the liquid phase. Solvent beads having air beads within the cutoff radius r_c were identified as candidates for removal. We defined the number of removed surface beads per time step as the evaporation rate. This study probes an evaporate rates range from 1 to 100 beads per time step. The simulation was terminated when all solvent beads were deleted and the polymer was considered to be solidified, resulting in the final morphology of the sprayed droplet. Notably, the DPD method simulates incompressible fluids and thus the total number density of the system must remain approximately constant. As a result, the simulation box is replenished with air beads as solvent beads are deleted. To avoid unphysical effect on the system dynamics, the new air beads were introduced only near the edge of the simulation box, away from the droplet.

Polymer skin formation

Fig. S2a confirms the development of a densified polymer skin at the surface of droplet, which was driven by the evaporation-induced advection.[16] This skin with much higher polymer concentration will naturally generate a pronounced viscosity gradient in the droplet. This result is consistent with the shell formation in a majority of sprays and also provides evidence that the bead-on-string morphology is associated with the presence of evaporation-driven viscosity gradient. Fig. S3a-c compares the final morphologies of dried polymer in simulations performed at different evaporation rates, in which the skin formation was also confirmed (Fig. S4). Consistent bead-on-string geometries were obtained.

Nanowire formation under suppressed evaporation

In experiments, the physical evaporation rate is typically much higher than the rates of mutual diffusion of polymer and solvent in the droplet. However, the evaporation rate is readily adjustable in the DPD simulation. This allows us to uniquely predict what will happen if the characteristic time scales of evaporation and diffusive processes are comparable. Fig. S2b shows that the polymer maintained its homogeneous distribution inside the droplet when evaporation was simulated at a much lower rate (*e.g.*, 1 bead per time step). No skin formation was observed under slow evaporation. In this regime, the formation of the Taylor cone pseudopods was inhibited, and the droplet only developed one filamentous protrusion during deformation, as shown in Supplementary Movie 3. The final geometry was nanowire (Fig. S2c). The entire morphology development resembles the one observed in Supplementary Movie 2 where the solvent was uniformly removed. These simulations provide strong evidence that the nanowire formation requires uniform droplet viscosity, while the presence of a significant viscosity gradient promotes the development of bead-on-string morphology.

References

1. Kovacevich, D. A. *et al.* Self-Limiting Electrospray Deposition for the Surface Modification of Additively Manufactured Parts. *ACS Appl. Mater. Interfaces* **12**, 20901–20911 (2020).
2. Groot, R. D. & Warren, P. B. Dissipative particle dynamics: Bridging the gap between atomistic and mesoscopic simulation. *J. Chem. Phys.* **107**, 4423–4435 (1997).
3. Español, P. & Warren, P. B. Perspective: Dissipative particle dynamics. *J. Chem. Phys.* **146**, 150901 (2017).
4. Pivkin, I. V, Caswell, B. & Karniadakisa, G. E. Dissipative Particle Dynamics. in *Reviews in Computational Chemistry* 85–110 (John Wiley & Sons, Inc., 2010). doi:10.1002/9780470890905.ch2.
5. Maiti, A. & McGrother, S. Bead–bead interaction parameters in dissipative particle dynamics: Relation to bead-size, solubility parameter, and surface tension. *J. Chem. Phys.* **120**, 1594 (2004).
6. Ginzburg, V. V., Chang, K., Jog, P. K., Argenton, A. B. & Rakesh, L. Modeling the Interfacial Tension in Oil−Water−Nonionic Surfactant Mixtures Using Dissipative

Particle Dynamics and Self-Consistent Field Theory. *J. Phys. Chem. B* **115**, 4654–4661 (2011).

7. Chen, S. & Yong, X. Dissipative particle dynamics modeling of hydrogel swelling by osmotic ensemble method. *J. Chem. Phys.* **149**, 094904 (2018).
8. Español, P. Hydrodynamics from dissipative particle dynamics. *Phys. Rev. E* **52**, 1734–1742 (1995).
9. Marsh, C. A., Backx, G. & Ernst, M. H. Static and dynamic properties of dissipative particle dynamics. *Phys. Rev. E* **56**, 1676–1691 (1997).
10. Boromand, A., Jamali, S. & Maia, J. M. Viscosity measurement techniques in Dissipative Particle Dynamics. *Comput. Phys. Commun.* **196**, 149–160 (2015).
11. Qin, S. & Yong, X. Interfacial adsorption of pH-responsive polymers and nanoparticles. *Soft Matter* **13**, 5137–5149 (2017).
12. Qin, S., Kang, J. & Yong, X. Structure and Dynamics of Stimuli-Responsive Nanoparticle Monolayers at Fluid Interfaces. *Langmuir* **34**, 5581–5591 (2018).
13. Qin, S. & Yong, X. Controlling the stability of Pickering emulsions by pH-responsive nanoparticles. *Soft Matter* **15**, 3291–3300 (2019).
14. Groot, R. D. Electrostatic interactions in dissipative particle dynamics—simulation of polyelectrolytes and anionic surfactants. *J. Chem. Phys.* **118**, 11265–11277 (2003).
15. Ibergay, C., Malfreyt, P. & Tildesley, D. J. Electrostatic interactions in dissipative particle dynamics: Toward a mesoscale modeling of the polyelectrolyte brushes. *J. Chem. Theory Comput.* **5**, 3245–3259 (2009).
16. Guenthner, A. J. *et al.* Dynamics of Hollow Nanofiber Formation During Solidification Subjected to Solvent Evaporation. *Macromol. Theory Simulations* **15**, 87–93 (2006).

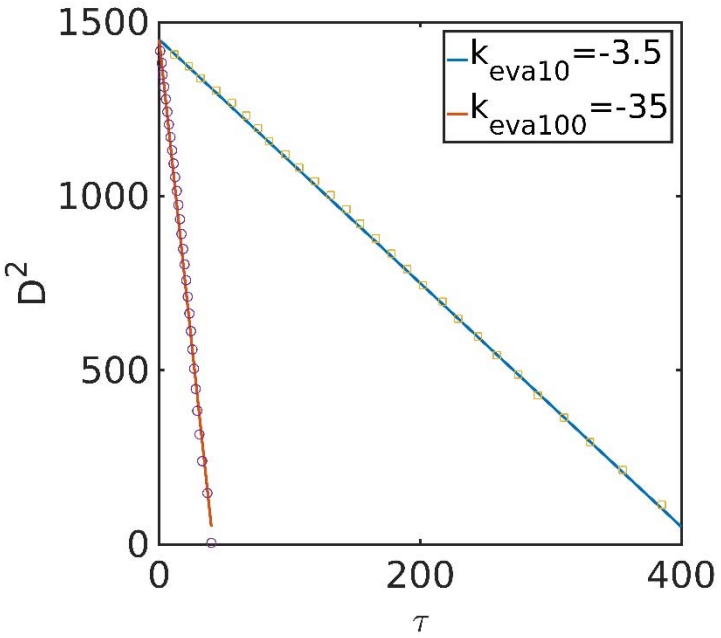

Fig. S1 Kinetics of simulated droplet evaporation. The square of the diameter of a pure solvent droplet under evaporation as a function of DPD simulation time. The rates of removing the solvent beads at the droplet surface are 10 and 100 beads per time step. The solid lines are linear fittings of the data, showing that the evaporation rate is proportional to the bead-removal rate.

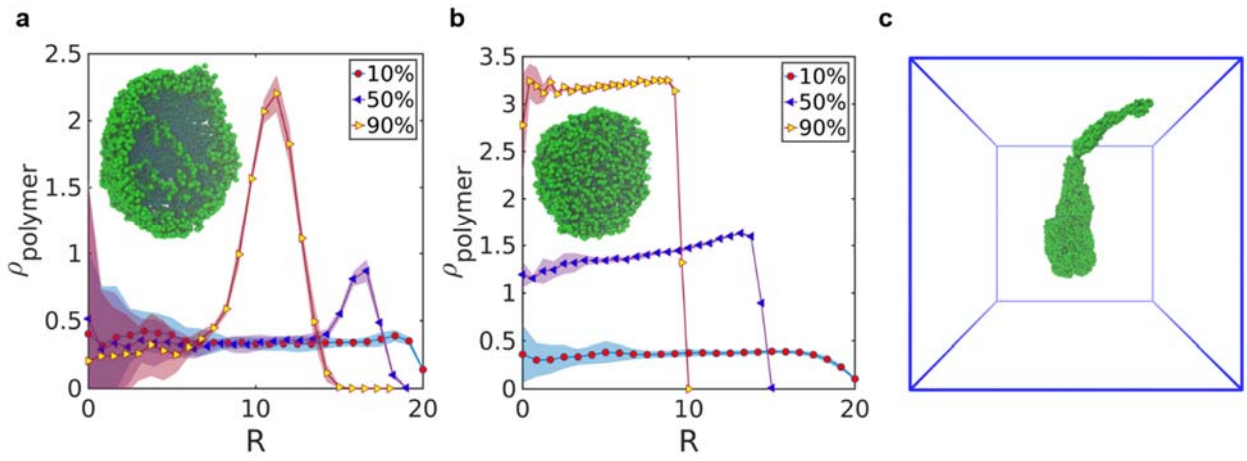

Fig. S2 Evolution of polymer density distribution during evaporation. (a, b) Radial polymer density profiles in the uncharged polymeric droplets in the DPD simulations at the instance when 10%, 50%, and 90% of solvent has been evaporated. The evaporation rates are (a) 100 and (b) 1 bead(s) per time step. The shaded error band represents the standard deviation of 5 independent runs. The insets are the corresponding cross-sectional snapshots of the droplet after evaporation of 90% of solvent. (c) Final morphology of the charged polymeric droplet obtained at the evaporation rate of 1 bead per time step.

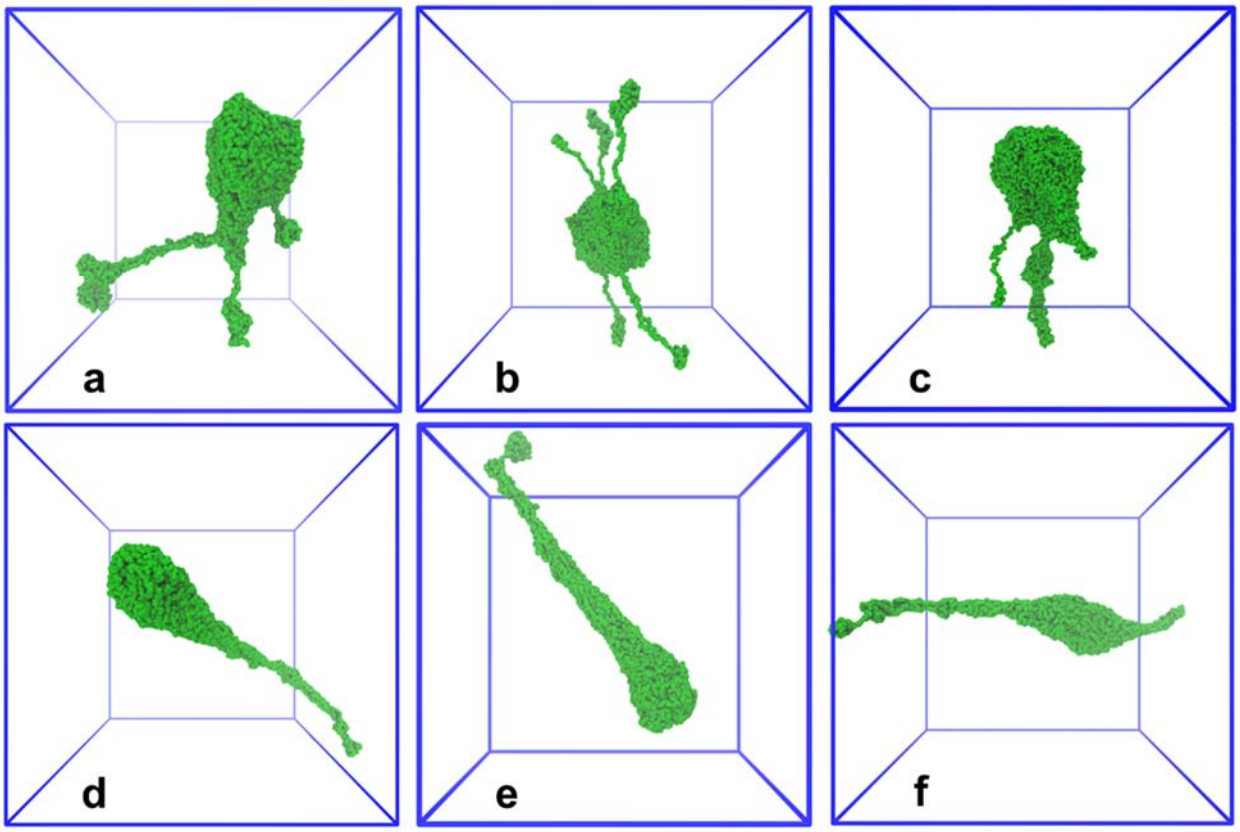

Fig. S3 Final droplet morphologies under different evaporation conditions. (a-c) Bead-on-string morphologies obtained under physical evaporation with rates of 10, 20, 50 beads per time step, respectively. (d-f) Consistent nanowires developed during homogeneous removal of the solvent beads at the rates of 3, 5, and 8 beads per time step, respectively. The green spheres are polymer beads. Vapor beads and ions are not shown for clarity.

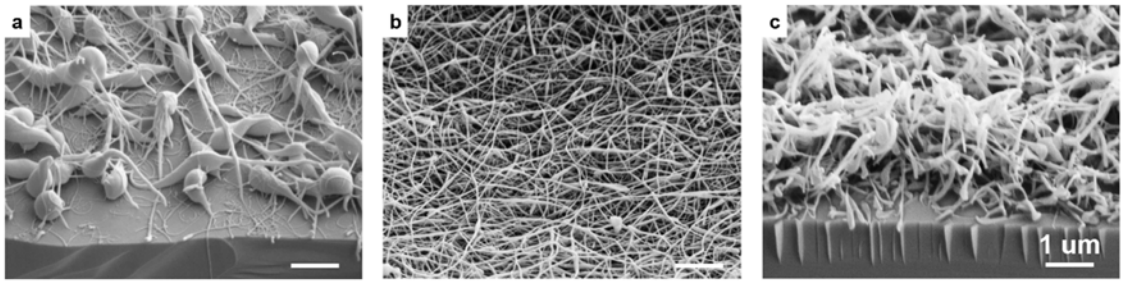

Fig. S4 SEM images of different gels spray. (a) 0.25 wt% PNIPAAm sprayed at substrate temperature of 25 °C from a 2:8 weight-basis water:ethanol blend; (b) 0.25 wt% gelatin sprayed at substrate temperature of 60 °C from 3:2 weight-basis water:ethanol blend; (c) 1 wt% HPMC sprayed at substrate temperature of 90 °C from 3:2 weight-basis water:ethanol blend. All sprays were conducted at the spray distance of 4 cm for 30 min at a flow rate of 0.1 mL/hr.

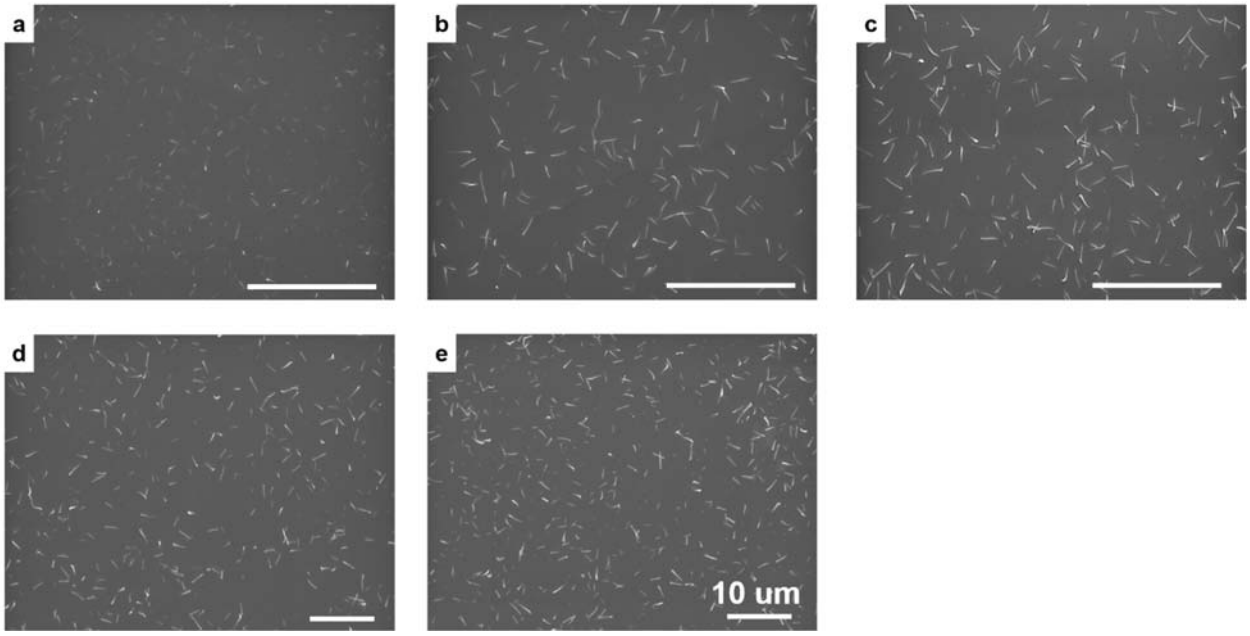

Fig. S5 SEM images of short time sprays of isolated single wires from 1 wt% MC sprayed in different flow rates: (a) 0.02 mL/hr, (b) 0.05 mL/hr, (c) 0.10 mL/hr, (d) 0.20 mL/hr, (e) 0.25 mL/hr. All sprays were conducted at a spray distance of 4 cm for 0.167 min and a substrate temperature of 90 °C from 3:2 weight-basis water-ethanol blend.

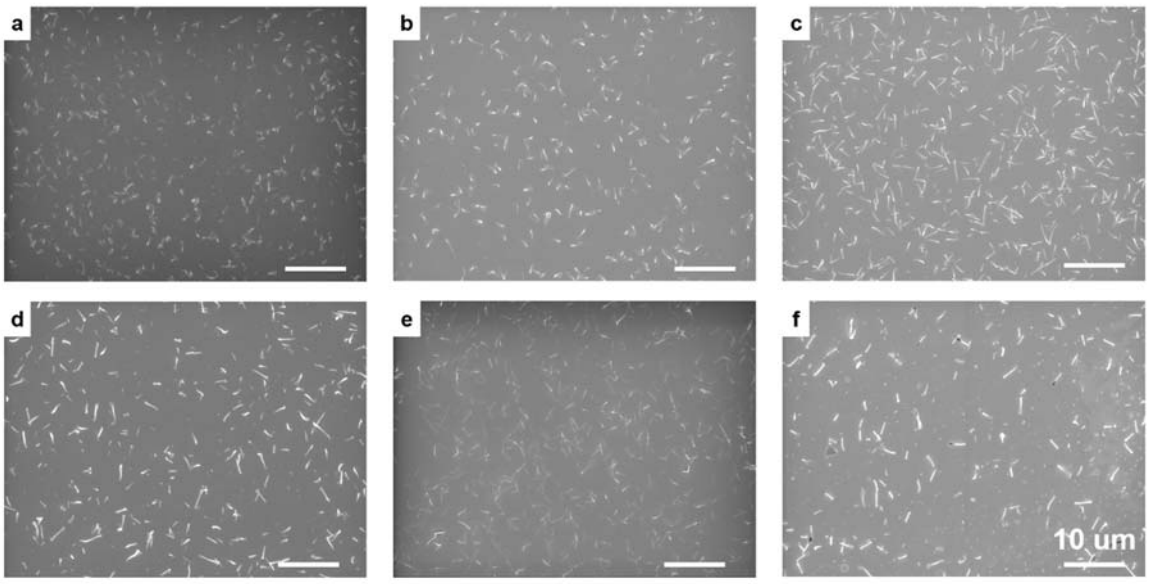

Fig. S6 SEM images of short time sprays of isolated single wires from MC of different loadings: (a) 0.125 wt% MC, (b) 0.25 wt% MC, (c) 0.5 wt% MC, (d) 1 wt% (5:1, MC:PEG 400), (e) 1 wt% (1:1, MC:PEG 400), (f) 2 wt% MC. All sprays were conducted at the spray distance of 4 cm for 0.167 min, with a spray flow rate of 0.25 mL/hr and a substrate temperature of 90 °C from 3:2 weight-basis water-ethanol blend.

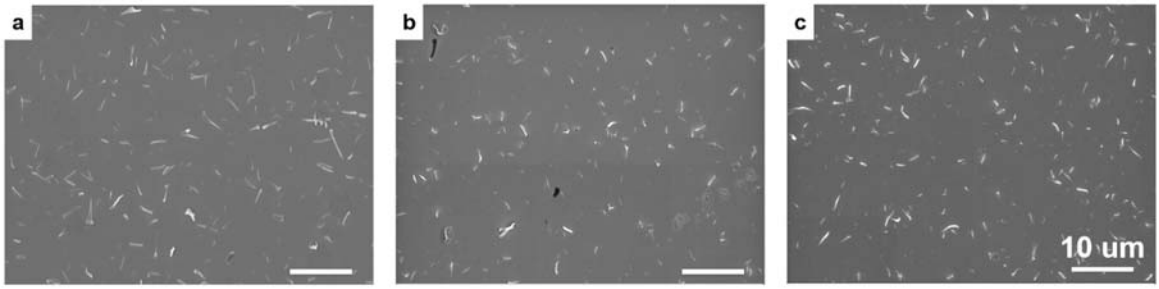

Fig. S7 SEM images of short time sprays of isolated single wires from 1 wt% MC of different molecular weights: (a) 17 kDa, (b) 41 kDa, (c) 63 kDa. All sprayed were conducted at the spray distance of 4 cm and a substrate temperature of 90 °C from 3:2 weight-basis water-ethanol blend. All sprays were conducted at a spray distance of 4 cm for 0.167 min and the substrate temperature of 90 °C from 3:2 weight-basis water-ethanol blend at the flow rate of 0.25 mL/hr.

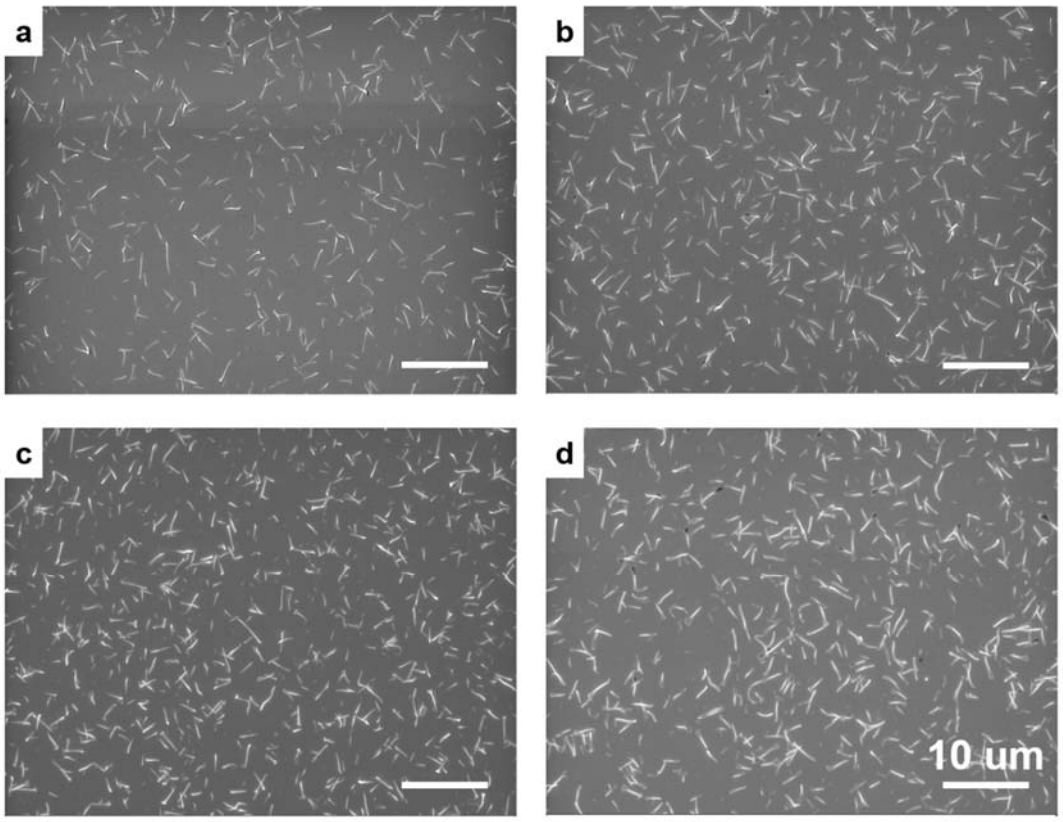

Fig. S8 SEM images of short time sprays of isolated single wires from 1 wt% MC of different spray distances: (a) 7 cm, (b) 6 cm, (c) 5 cm, (d) 3 cm. All sprays were conducted at a flow rate of 0.25 mL/hr for 0.167 min and a substrate temperature of 90 °C from 3:2 weight-basis water-ethanol blend.

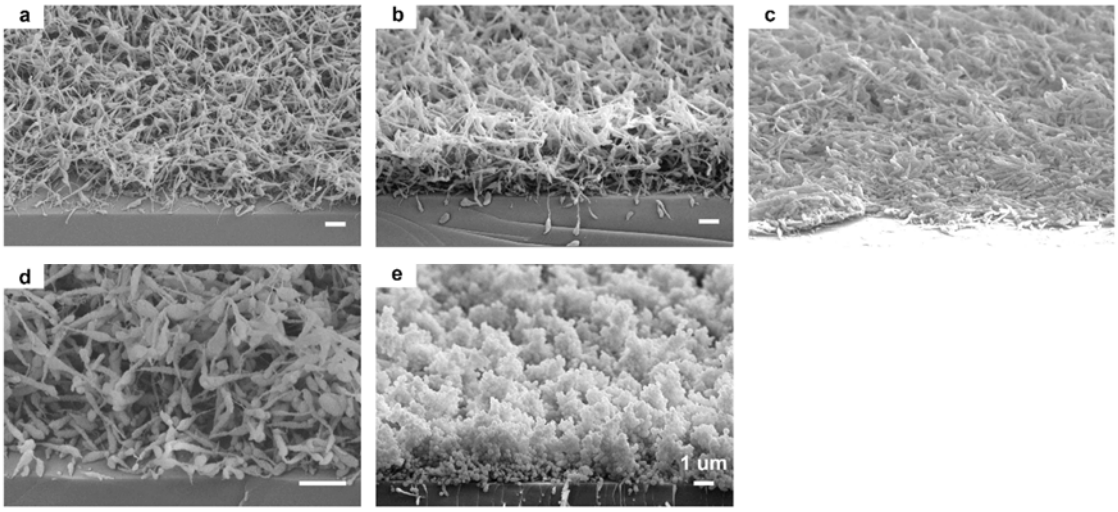

Fig. S9 SEM images of 1 wt% MC:silica particles sprayed in different ratios: (a) 5:1; (b) 1:1; (c) 1:2; (d) 1:5; (e) 0:1. All sprays were conducted from 3:2 weight-basis water-ethanol blend, the spray distance of 4 cm in the flow rate of 0.25 mL/hr with a substrate temperature of 90 °C. (a-d) were sprayed for 60 min, (e) was sprayed for 100 min.

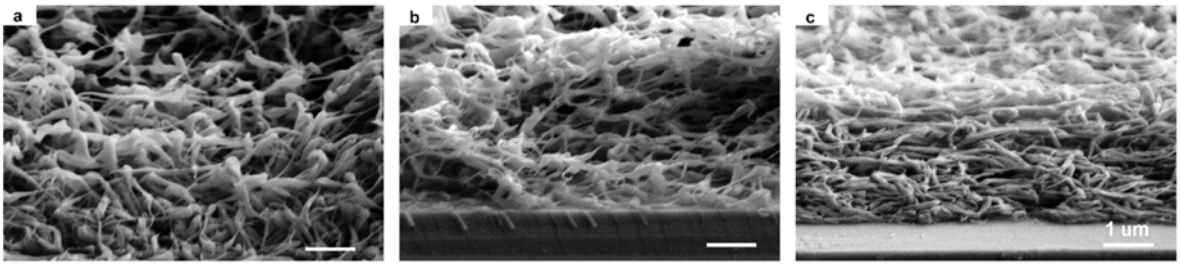

Fig. S10 SEM images of 1 wt% MC:EG sprayed in different ratios: (a) 5:1; (b) 3:1; (c) 1:1. All sprays were conducted from 3:2 weight-basis water-ethanol blend, the spray distance of 4 cm and the flow rate of 0.25 mL/hr with a substrate temperature of 90 °C for 60 min.

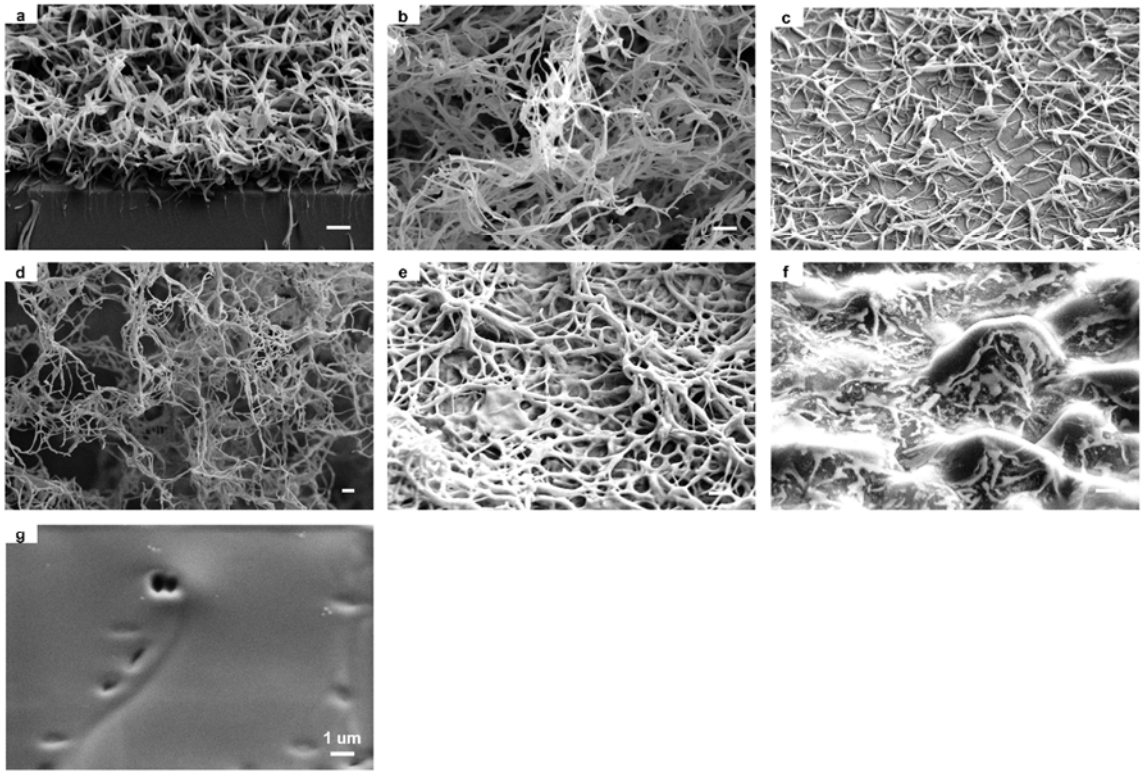

Fig. S11 SEM images of 1 wt% MC:PEG 400 sprayed in different ratios: (a) 1:0; (b) 5:1; (c) 2:1; (d) 1:1; (e) 1:2; (f) 1:5; (g) 0:1. All sprays were conducted from 3:2 weight-basis water-ethanol blend, the spray distance of 4 cm in the flow rate of 0.25 mL/hr with a substrate temperature of 90 °C for 30 min.

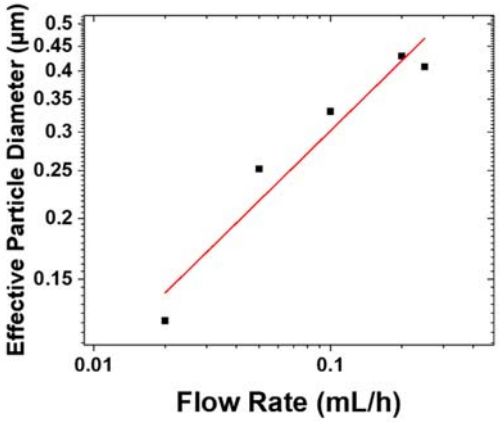

Fig. S12 Linear fit on a log-log scale of particle diameter as a function of flow rate for particles having the same volume as a cylinder with the diameter and length of the mean NWs in the flow rate series. The fit has a slope of 0.48, an *x*-intercept of -0.04, and an R^2 value of 0.94.

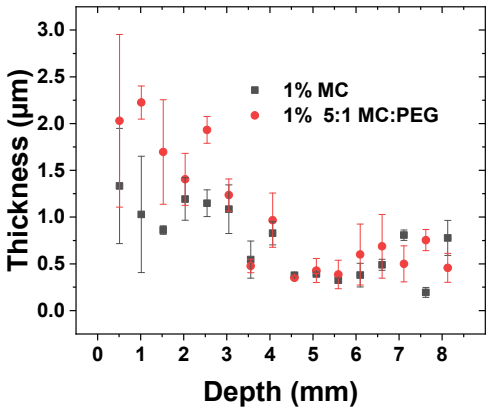

Fig. S13 Average of four thickness measurements from holes of different depth of smoothed MC (black) and MC:PEG 400 (5:1) sprays. Sprays were conducted without a focusing ring at 8 kV of potential, a flow rate of 0.25 mL/hr, a spray distance of 4 cm, 6 cm vertical, and a spray substrate temperature of 90 °C for 5.5 hours. Penetration into the deeper holes is indicative of a self-limiting electrospray deposition.

Morphology		Sprayed Materials	Citation
Particles	1	Poly(ethylene oxide)	Morota, K.; Matsumoto, H.; Mizukoshi, T.; Konosu, Y.; Minagawa, M.; Tanioka, A.; Yamagata, Y.; Inoue, K. *Journal of colloid and interface science* **2004,** 279, (2), 484-492.
	2	Poly(acrylic acid), poly(allylamine)	Altmann, K.; Schulze, R.-D.; Friedrich, J. *Thin solid films* **2014,** 564, 269-276.
	3	Poly(vinylidene fluoride)	Rietveld, I. B.; Kobayashi, K.; Yamada, H.; Matsushige, K. *Journal of colloid and interface science* **2006,** 298, (2), 639-651.
	4	Poly(2-hydroxyethyl methacrylate-co-MAA)	Mizukoshi, T.; Matsumoto, H.; Minagawa, M.; Tanioka, A. *Journal of applied polymer science* **2007,** 103, (6), 3811-3817.
	5	Poly(vinyl pyrrolidone), carbamazepine	Kawakami, K. *International journal of pharmaceutics* **2012,** 433, (1-2), 71-78.
	6	Poly(vinylidene fluoride)	Rietveld, I. B.; Kobayashi, K.; Yamada, H.; Matsushige, K. *Soft Matter* **2009,** 5, (3), 593-598.
	7	Poly (d, l-lactide-co-glycolic acid)	Rezvanpour, A.; Wang, C.-H. *Chemical engineering science* **2011,** 66, (17), 3836-3849.
	8	Poly(lactic-co-glycolic acid), metronidazole	Hao, S.; Wang, Y.; Wang, B.; Deng, J.; Zhu, L.; Cao, Y. *Materials Science and Engineering: C* **2014,** 39, 113-119.
	9	Poly(lactic-co-glycolic acid), lactic and glycolic monomers	Almería, B.; Gomez, A. *Journal of colloid and interface science* **2014,** 417, 121-130.
	10	Poly(lactic acid)	Ikeuchi, M.; Tane, R.; Ikuta, K. *Biomedical microdevices* **2012,** 14, (1), 35-43.

	11	Poly(styrene), Kraton® D1102, oligomeric silsesquioxane	Lei, L.; Kovacevich, D. A.; Nitzsche, M. P.; Ryu, J.; Al-Marzoki, K.; Rodriguez, G.; Klein, L. C.; Jitianu, A.; Singer, J. P. *ACS applied materials & interfaces* **2018,** 10, (13), 11175-11188.
	12	Poly(acrylonitrile), poly(vinyl alcohol), Triton X-100	You, H.; Yang, Y.; Li, X.; Zhang, K.; Wang, X.; Zhu, M.; Hsiao, B. S. *Journal of membrane science* **2012**, 394, 241-247.
Wire-mats	1	Polyvinylidene fluoride, poly(methyl methacrylate)	Nasir, M.; Matsumoto, H.; Minagawa, M.; Tanioka, A.; Danno, T.; Horibe, H. *Polymer journal* **2009,** 41, (5), 402-406.
	2	Poly(2-hydroxyethyl methacrylate-co-methacrylic acid)	Matsumoto, H.; Mizukoshi, T.; Nitta, K.; Minagawa, M.; Tanioka, A.; Yamagata, Y. *Journal of colloid and interface science* **2005,** 286, (1), 414-416.
	3	Poly(ethylene-co-vinyl acetate), poly(lactic acid)	Kenawy, E.-R.; Bowlin, G. L.; Mansfield, K.; Layman, J.; Simpson, D. G.; Sanders, E. H.; Wnek, G. E. *Journal of controlled release* **2002,** 81, (1-2), 57-64.
	4	Poly(3-hexylthiophene-2,5-diyl) with [6,6]-phenylC_{61}-butyric acid methylester	Liao, Y.; Fukuda, T.; Takagi, K.; Kamata, N.; Fukuda, F.; Furukawa, Y. *Thin Solid Films* **2014,** 554, 132-136.
Worm-like rings	1	Poly(lactic-co-glycolic acid)	Almería, B.; Gomez, A. *Journal of colloid and interface science* **2014,** 417, 121-130.
	1	Paclitaxel, Poly (D,L-lactide-co-glycolic acid)	Xie, J.; Tan, J. C.; Wang, C.-H. *Journal of pharmaceutical sciences* **2008,** 97, (8), 3109-3122.

Films	2	α-Lactalbumin	Uematsu, I.; Matsumoto, H.; Morota, K.; Minagawa, M.; Tanioka, A.; Yamagata, Y.; Inoue, K. *Journal of colloid and interface science* **2004,** 269, (2), 336-340.
	3	/	Hu, H.; Gopinadhan, M.; Osuji, C. O. *Soft matter* **2014,** 10, (22), 3867-3889.
	4	Poly(styrene)-b-poly(ethylene oxide)	Hu, H.; Rangou, S.; Kim, M.; Gopalan, P.; Filiz, V.; Avgeropoulos, A.; Osuji, C. O. *ACS nano* **2013,** 7, (4), 2960-2970.
	5	/	Hu, H.; Toth, K.; Kim, M.; Gopalan, P.; Osuji, C. O. *MRS Communications* **2015,** 5, (2), 235-242.
	6	poly(styrene-b-4-vinylpyridine)	Hu, H.; Singer, J. P.; Osuji, C. O. *Macromolecules* **2014,** 47, (16), 5703-5710.

Flakes[†]	1	Pt/C + Nafion	Chaparro, A.; Folgado, M.; Ferreira-Aparicio, P.; Martín, A.; Alonso-Álvarez, I.; Daza, L. *Journal of The Electrochemical Society* **2010,** 157, (7), B993-B999.
	2	CsH_2PO_4, Pt on carbon, Poly(vinyl pyrrolidone)	Varga, Á.; Brunelli, N. A.; Louie, M. W.; Giapis, K. P.; Haile, S. M. *Journal of Materials Chemistry* **2010,** 20, (30), 6309-6315.

Table S1. A limited collection of observed morphologies from electrospray deposition.

[†] The formation of flakes appears to arise from crystallization of the deposited material and is somewhat distinct from the phenomena discussed here.

	Concentration (wt%)	Ratio	Flow Rate (mL/hr)	Molecular Weight (kDa)	Temperature (°C)	Distance (cm)	Solvent (W/E)	Spray Voltage (kV)	Focus Voltage (kV)	Spray Time (min)	Humidity (%)
MC Temperature Series	1	/	0.25	14	30	4	3/2	6.2	2.5	30	65-70
					50			6.2	2.8		55-60
					70			6.2	2.8		55-60
					90			6.2	1.8		29
					110			6.2	2.8		55-60
MC Time Series	1	/	0.25	14	90	4	3/2	6.2	2.8	15	55-60
								6.2	2.8	30	55-60
								6.2	2.8	60	55-60
								6.2	2.8	90	55-60
								6.2	2.8	120	55-60
MC Flow Rate Series	1	/	0.02	14	90	4	3/2	6.2	5.2	225	43
			0.05					6.2	3.0	90	43
			0.15					6.2	2.3	30	43
			0.25					6.2	2.8	18	43
			0.35					6.2	1.8	12.86	43
MC Spray Distances Series	1		0.25	14	90	7	3/2	10.8	8.4	30	23
						6		9.3	7.8		23

						5		7.8	4.0		23
						3		4.7	0.3		20
MC:EG	1	5:1	0.25	14	90	4	3/2	6.2	2.2	60	63
		3:1						6.2	2.2		53
		2:1						6.2	2.2		58
		1:1						6.2	2.2		48
MC:Silica Nanoparticles	1	5:1	0.25	14	90	4	3/2	6.2	2.5	60	50-55
		2:1						6.0	2.0		51-53
		1:1						6.2	2.4		51-53
		1:2						6.2	2.2		51-53
		1:5						6.2	2.8		51-53
		0:1						6.2	3.0	100	50-55
MC:PEG 400	1	5:1	0.25	14	90	4	3/2	6.2	3.3	30	25
		2:1						6.2	3.3		24
		1:1						6.2	3.3		25
		1:2						6.2	3.5		25
		1:5						6.2	3.5		24
		0:1						6.2	5.1		24
MC:50 nm Gold Nanoparticles	0.3	0:1	0.15	14	90	4	3/2	6.2	3.3	30	15-20
		1:5						6.2	2.5		15-20

		1:2						6.2	3.0		15-20
		1:1						6.2	2.7		15-20
		2:1						6.2	2.5		15-20
		5:1						6.2	2.8		15-20
		1:0						6.2	2.5		15-20
(5:1) (MC:PEG 400) : 50 nm Gold Nanoparticles	0.3	0:1	0.15	14	90	4	3/2	6.2	3.3	30	18
		1:5						6.2	2.7		18
		1:2						6.2	2.8		18
		1:1						6.2	2.9		18
		2:1						6.2	2.5		18
		5:1						6.2	2.5		18
		1:0						6.2	2.5		18
MC Flow Rate Series Single Wire	1	/	0.02	14	90	4	3/2	6.2	5.2	0.167	45
			0.05					6.2	3.0		45
			0.10					6.2	2.3		45
			0.20					6.2	2.8		45
			0.25					6.2	1.8		45
MC Concentration Series Single Wire	0.125	/	0.25	14	90	4	3/2	6.2	2.9	0.167	45
	0.25							6.2	2.4		45
	0.5							6.2	2.2		45

	2							6.2	2.2		45
	1 (MC:PEG 400)	5:1						6.2	2.6		45
		1:1						6.2	3.3		25
MC Molecular Weight Series Single Wire	1	/	0.25	14	90	4	3/2	6.2	2.3	0.167	45
				17				6.2	2.6		45
				41				6.2	3.0		45
				63				6.2	2.5		45
MC Spray Distances Series Single Wire	1	/	0.25	14	90	7	3/2	10.8	8.4	0.167	23
						6		9.3	7.8		23
						5		7.8	4.0		23
						3		4.7	0.3		20
PNIPAAm	0.25	/	0.10	/	25	4	3/2	6.5	/	30	23
Gelatin	0.25				60			6.4	/		23
HPMC	1				90			6.2	2.5		23
MC 4X4 hole array of depth	1	/	0.25	14	90	4 (horizontal)	3/2	8.0	/	330	40
MC:PEG 400 4X4 hole array of depth	1	5:1	0.25	14	90	6 (vertical)	3/2	8.3	/	330	40

3D Tree (5:1) (MC:PEG 400) : 50 nm Gold Nanoparticles	1	5:1	0.20	14	25	3 (horizontal) 4 (vertical)	3/2	7.4	/	1800	40

Table S2. Experimental parameters for electrospray samples.

Movie S1.

Bead-on-string morphology of a sprayed polymer droplet developed in the simulation under physical evaporation at a rate of 100 beads per time step.

Movie S2.

Polymer nanowire formation in the simulation with random removals of solvent beads at a rate of 2 beads per time step.

Movie S3.

Polymer nanowire formation in the simulation under physical evaporation at a rate of 1 bead per time step.

Movie S4.

2000X time lapse video of gold nanoparticles being sprayed on a Thoweil Hinoki Cypress